Effect of compactification of twisted toroidal extra-dimension on sterile neutrino

A. K. Mohanty*
Saha Institute of Nuclear Physics, Kolkata - 700064 and Bhabha Atomic Research Centre, Mumbai-400084, INDIA
(Dated: June 27, 2016)

We consider a toroidal extra-dimensional space with shape moduli θ which is the angle between the two large extra dimensions R_1 and R_2 (twisted LED with $\delta = 2$). The Kaluza-Klein (KK) compactification results in a tower of KK bulk neutrinos which are sterile in nature and couple to the active neutrinos in the brane. The active-sterile mixing probability strongly depends on the angle θ due to changing pattern of KK mass gaps which leads to level crossing. Considering only the first two lowest KK states in analogy with $(3+2)$ model, it is shown that $|U_{\alpha 4}| > |U_{\alpha 5}|$ when $\theta = \pi/2$ corresponding to the case of a normal torus. Since $\Delta^2_{14} < \Delta^2_{15}$, this is expected in normal LED model as higher the sterile mass lower is the mixing probability. Contrary to this expectation, it is found that there exists a range in θ where $|U_{\alpha 5}| \geq |U_{\alpha 4}|$ even though $\Delta m^2_{14} < \Delta m^2_{15}$ which has been demonstrated qantitatively using fourier transformation of reactor anti-neutrino spectrum. This is an important observation which can be linked to the oscillation parameters extracted by several $(3+2)$ global analyses of the neutrino and anti-neutrino data obtained from the short base line measurements.

PACS numbers:

arXiv:1606.07625v1 [hep-ph] 24 Jun 2016

I. INTRODUCTION

We consider the compactification of toroidal two extra dimensions characterised by a shape moduli θ which is the angle bewteen the two large extra dimensions R_1 and R_2. The non trivial effect of shape moduli on compactification was first studied by Dienes and Mafi who brought out a number of profound phenomena relevant for the interpretation of experimental data if such extra dimensions exist [1, 2]. Notably among them is the changing pattern of Kaluza-Klein (KK) mass gaps which strongly depend on θ and exhibit level crossing making some of the higher KK modes lighter as compared to the lower ones when θ is varied. This is an important aspect which we incorporate in the ADD (Arkani-Hamed, Dimopoulos and Dvali) model with two large extra dimensions (LED) to study the active-sterile neutrino mixing in $4+\delta$ dimensions with $\delta = 2$ [3, 4]. Another impetus to this work stems from the recent observation that the fit to the short base line (SBL) reactor anti-neutrino measurements with new anti-neutrino flux [5, 6] improves considerably if two sterile neutrions $(3+2)$ are assumed instead of one $(3+1)$ [7]. Naively, it is observed that Δm_{51} is about $\sqrt{2}$ times larger than Δm_{41} and $|U_{15}| \geq |U_{14}|$ [7, 8]. The LED model with $\delta = 1$ (one extra dimension larger than others) results in a tower of KK sterile neutrions with KK mass increasing as n and mixing probability decreasing as $1/n^2$ where $n = 1, 2, 3$ etc [9–18]. Obviously, the case with $\delta = 1$ is not consistent with the above observations if we consider first two lowest sterile states. In case of $\delta = 2$, the KK mass increases as $\sqrt{m^2 + n^2}$ where m and n are two different KK modes associated with R_1 and R_2 respectively. Although the mass of first two KK modes $(1, 0)$ or $(0, 1)$ and $(1, 1)$ differ by a factor of $\sqrt{2}$, as expected, still it does not predict the observed active-sterile mixing probability when $\theta = \pi/2$. On the other hand, when θ is close to $\pi/4$, the predicted masses and mixing probabilities are found to be consistent with the above experimental obsevations. In this letter, we consider compactification on a general two-torus corresponding to $\delta = 2$ instead of $\delta = 1$ as one dimensional compactification lacks shape moduli. It is shown here that there exists a range in θ where $|U_{\alpha 5}| \geq |U_{\alpha 4}|$ even though $\Delta m^2_{14} < \Delta m^2_{15}$. This is an important observation which is demonstrated more quantitatively using cosine Fourier transformation of the reactor anti-neutrino spectra.

II. FORMALISM

We consider a brane world theory with 6 dimensional bulk, where the active neutrinos are confined to the brane and the singlet sterile neutrino $\Phi^\alpha(x^\mu, y_1, y_2)$ propagates in the bulk with extra dimensions y_1 and y_2. Using the Kaluza-Klein (KK) expansion, the singlet fermionic field can be expanded as,

*Electronic address: ajitkumar.mohanty@saha.ac.in

$$\Phi_{R/L}(x^{\mu}, y) \sum_{m} \sum_{n} \Phi_{R/L}^{(m,n)}(x^{\mu})\ f^{mn}(y_1, y_2), \tag{1}$$

where $\mu = 0, 1, 2, 3$ are co-ordinates belonging to the brane and $y_1,\ y_2$ are the co-ordinates of two extra dimensions. The subscripts R and L refer explicitly to four dimensional Lorentz property. The periodic function $f^{mn}(y_1, y_2)$ is given by,

$$f^{mn}(y_1, y_2) = \frac{1}{\sqrt{V}} exp\left[i \frac{m}{R_1} \left(y_1 - \frac{y_2}{tan\theta} \right) + i \frac{n}{R_2} \frac{y_2}{sin\theta} \right], \tag{2}$$

with periodicity $y_1 \sim y_1 + 2\pi(R_1 + R_2 cos\theta)$ and $y_2 \sim y_2 + 2\pi R_2 sin\theta$ [1]. The normalization factor $V = 4\pi^2 R_2 sin\theta (R_1 + R_2 cos\theta)$ plays the role of volume of the extra-dimensions. Note that for $\theta = \pi/2$, $V = 4\pi^2 R_1 R_2$ which is the volume of a normal torus. Eq. 2 satisfies the condition,

$$\frac{1}{V} \int_0^{\infty} (f^{pq})^*\ f^{mn} dy_1 dy_2 = \delta_{pm} \delta_{qn}. \tag{3}$$

The bulk action responsible for the neutrino mass is given by (kinetic term is not included) [19],

$$A_{bulk} = \int d^4x\ dy_1\ dy_2\ \left[\Phi_L^{\dagger} (\partial_5 + i\partial_6) \Phi_R - \Phi_R^{\dagger} (\partial_5 - i\partial_6) \Phi_L \right]. \tag{4}$$

Using Eq. 1, Eq. 2, Eq. 3 and the substitution,

$$\Psi_R^{0,0} = \Phi_R^{0,0} \quad ; \quad \Psi_R^{m,n} = \frac{1}{\sqrt{2}} \left(\Phi_R^{m,n} + \Phi_R^{-m,-n} \right) \quad ; \quad \Psi_L^{m,n} = \frac{1}{\sqrt{2}} \left(\Phi_L^{m,n} + \Phi_L^{-m,-n} \right), \tag{5}$$

the y_1 and y_2 variable in Eq. 4 can be integrated out to get,

$$A_{bulk} = -\int d^4x \sum_{m,n}^{N} \frac{k_{m,n}}{R} \left(\Psi_R^{(m,n)\dagger} \Psi_L^{(m,n)} + \Psi_L^{(m,n)\dagger} \Psi_R^{(m,n)} \right), \tag{6}$$

where the absolute value of the mass term for (m, n) mode is given by,

$$k_{m,n} = \sqrt{\frac{1}{sin\theta} (m^2 + n^2 - 2m\ n\ cos\theta)}. \tag{7}$$

We have relaxed the condition further by assuming that $R_1 = R_2 = R$. Note that the summation $\sum_{mn}$ above is over all modes of m and n upto a maximum value of N, but excluding $m = n = 0$ mode. We can now add the relevant portion of interaction term between brane and the bulk field containg mass,

$$A_{int} = -m_D \int d^4x \left[\nu_L^{\dagger} \left(\nu_R + \sqrt{2} \sum_{m,n}^{N} \Psi_R^{(m,n)} \right) + hc \right] \tag{8}$$

where $\nu_R = \Psi_R^{(0,0)}$ and m_D is the Dirac neutrino mass generated due to coupling of bulk neutrinos with the brane localized SM Higgs boson at $y_1 = y_2 = 0$. Finally, by collecting the neutrino mass terms in the Lagrangian and explicitly including the neutrino flavor indices α and β, we obtain,

$$\mathcal{L}_{mass} = -\sum_{\alpha=1}^{3} \sum_{m,n}^{N} \frac{k_{m,n}}{R} \Psi_R^{\alpha(m,n)\dagger} \Psi_L^{\alpha(m,n)} - \sum_{\alpha,\beta=1}^{3} m_D^{\alpha\beta} \left(\nu_R^{\alpha\dagger} + \sqrt{2} \sum_{m,n}^{N} \Psi_R^{\alpha(m,n)\dagger} \right) \nu_L^{\beta} + hc \tag{9}$$

Note that while the right handed sterile neutrino $\Psi_R^{0,0}$ participates in the process of mass generation at the brane, the left handed sterile neutrino $\Psi_L^{0,0}$ decouples from the mass part of the Lagrangian as k_{mn} vanishes for $(0,0)$ mode. We also neglect the Majrona mass and associate suitable lepton number to Ψ_R so that lepton number is conserved. The formalism is now similar to the case of $\delta = 1$ and can be found in several works [9–18]. Therefore, following the standard procedure of diagonalizing the Dirac mass term $m^{\alpha\beta}$ with PMNS matrx U and making a symmetric transformation to a set of new basis, the mass Lagrangian can be written in a compact form given by [11, 16],

$$\mathcal{L}_{mass} = \frac{1}{2}\bigg(\nu^\dagger M\nu + hc\bigg), \tag{10}$$

where the neutrino mass matrix M is given by,

$$M = \begin{pmatrix} 0 & m_\nu & m_\nu & m_\nu & m_\nu & \cdots & m_\nu \\ m_\nu & 0 & 0 & 0 & 0 & \cdots & 0 \\ \vdots & \vdots & \vdots & \vdots & \vdots & \vdots & \vdots \\ m_\nu & 0 & \frac{k_{mn}}{R} & 0 & 0 & \cdots & 0 \\ m_\nu & 0 & 0 & -\frac{k_{mn}}{R} & 0 & \cdots & 0 \\ \vdots & \vdots & \vdots & \vdots & \vdots & \vdots & \vdots \\ m_\nu & 0 & 0 & 0 & \cdots & \frac{k_{NN}}{R} & 0 \\ m_\nu & 0 & 0 & 0 & 0 & \cdots & -\frac{k_{NN}}{R} \end{pmatrix}, \tag{11}$$

with $\nu = (\nu_L, \nu_R, \nu_s^{-1}, \nu_s^1 \cdots)^T$. In the above, the Dirac mass m_ν could be either m_1, m_2 or m_3 depending on whether it is e, μ or τ neutrino. The mass term k_{mn}/R appearing in Eq. 11 represents $(d_k \times d_k)$ block diagonal matrix, d_k being the degeneracy of the (m,n) mass state, N is the upper limit of m or n. For $N = 1$, the independent modes are $(1,0)$ and $(1,1)$ since $(0,1)$ and $(1,0)$ mode degenerates. Similarly for $N = 2$, the independent modes are $(0,1)_{d=2}$, $(1,1)$, $(2,0)_{d=2}$, $(1,2)_{d=2}$ and $(2,2)$. Therefore, for the case of $\delta = 2$, d is either 2 or 1. Finally, we will make a distinction between k_{mn} and k which will be used interchangably in the following. The k_{mn} represents a mass state as defined in Eq. 7 for a given (m,n) mode where as the index k represents the k^{th} state. In the above example of $N = 2$, the six states including a $(0,0)$ mode can be represented by the index $k = 0,1,2,3,4,5$ and each state having mass given by k_{mn} with degeneracy d_k.

III. EIGEN VALUE AND EIGEN VECTOR

The eigen value λ of Eq. 11 can be obtained from the characteristic equation, $Det(M - \lambda I) = 0$ given by [16],

$$\bigg[\prod_{m,n}^{N}\bigg(\frac{k_{mn}^2}{R^2} - \lambda^2\bigg)^{d_k}\bigg]\bigg[\lambda^2 - m_\nu^2 + 2\lambda^2 m_\nu^2 \sum_{m,n}^{N}\frac{d_k}{\frac{k_{mn}^2}{R^2} - \lambda^2}\bigg] = 0. \tag{12}$$

There are $(d_k - 1)$ states for which λ is equal to k_{mn}/R and one state for which k_{mn} is not equal to k_{mn}/R for which the solutions can be obtained from,

$$\bigg[\lambda^2 - m_\nu^2 + 2\lambda^2 m_\nu^2 \sum_{m,n}^{N}\frac{1}{\frac{k_{mn}^2}{R^2} - \lambda^2}\bigg] = 0. \tag{13}$$

In Eq. 13, the factor d_k is not included explicitly as the summation over (m,n) takes care of it. Unlike $\delta = 1$ case, the summation in the above equation is logarithmically divergent. Therefore, we solve for a given λ_k iteratively up to a cut-off scale set by k_{NN}/R.

The matrix Eq. 11 can also be diagonalised by the unitary matrix L whose k^{th} column matrix corresponding to the mode (m,n) is given by,

$$L^k = \frac{1}{\sqrt{B}}\bigg(1, \frac{m_\nu}{\lambda_k}, \cdots, \frac{m_\nu}{\lambda_k - \frac{1}{R}}, \frac{m_\nu}{\lambda_k + \frac{1}{R}}, \cdots, \frac{m_\nu}{\lambda_k - \frac{k_{mn}}{R}}, \frac{m_\nu}{\lambda_k + \frac{k_{mn}}{R}}, \cdots, \frac{m_\nu}{\lambda_k - \frac{k_{NN}}{R}}, \frac{m_\nu}{\lambda_k + \frac{k_{NN}}{R}}\bigg)^T \tag{14}$$

The normalization factor B is obtained from the condition $(L^k)^T L^k = 1$.

The neutrino state of a given flavor ν_L^α can be written in terms of mass eigen states as,

$$\nu_L^\alpha = \sum_{j=1}^{3} U^{\alpha j} \sum_k L_j^{0k} \nu_L'^{j(k)}, \tag{15}$$

where $(L_j^{0k})^2 = 2/B$. A quantity of crucial interest is the survival probability of neutrino of flavor α after travelling a distance of L is given by [14],

$$P_{\alpha\alpha}(L) = \left| \sum_{j=1}^{3} \left|U^{\alpha j}\right|^2 \sum_k (L_j^{0k})^2 exp\left(i \frac{2.54 \lambda_j^{(k)2} L}{E_\nu}\right) \right|^2, \tag{16}$$

where E_ν is the neutrino energy in MeV, the eigen value λ_j is in eV and L is in m. In Eq. 16, the subscript $j = 1, 2, 3$ refers to e, μ, τ respectively.

In analogy with $(3+n)$ model, we can define another parameter of interest $S_{\alpha k}$ as,

$$S_{\alpha k} = \sum_{j=1}^{3} \left|U_{\alpha j} L_j^{0k}\right|^2, \tag{17}$$

so that we can identify the parameters $S_{\alpha 1}$ and $S_{\alpha 2}$ with either $|U_{\alpha 4}|^2$ or $|U_{\alpha 5}|^2$. Note that in the absence of extra dimensions, $S_{\alpha 0}$ is equal to unity since PMNS matrix is unitary. However, it is less than unity when L_j^{0k} is included. For neutrino mass square differences, we use $\Delta m_{21}^2 = 7.45 \times 10^{-5}\ eV^2$, $\Delta m_{31}^2 = 2.417 \times 10^{-3}\ eV^2$ [20]. In the normal hierarchy (NH: $m_3 > m_2 > m_1$), we consider m_1 as a variable and express ${m_2}^2 = m_1^2 + \Delta m_{21}^2$ and $m_3^2 = m_2^2 + \Delta m_{31}^2$ respectively. In the inverted hierarchy (IH: $m_2 > m_1 > m_3$), m_3 is considered as a variable and express $m_2^2 = m_3^2 + \Delta m_{32}^2$ and $m_1^2 = m_3^2 + \Delta m_{31}^2$ respectively. Other parameters are $sin^2\theta_{12} = 0.313$, $sin^2\theta_{23} = 0.444$ and $sin^2\theta_{13} = 0.0244$ respectively [20].

The fig. 1 shows the plot of eigen values $\lambda_k R$ as a function of mass m_1 for $N = 1, 2, 9$ (other masses are fixed based on NH) solved iteratively using the Eq. 13. The eigen value λ_k is defined as the average $\frac{1}{3}\sum_j \lambda_k^j$. It is easy to check that Eq. 13 has large number of solutions λ_k depending on the m , n and N values, although shown for only $(0,0)$, $(1,0)$ and $(1,1)$ modes only since $(0,1)$ and $(1,0)$ modes are degenerate. As can be seen, the solutions are not convergent due to logarithmic divergent and strongly depend on the choice of cut-off value N particularly for large m_1 values. However, for small m_1 (more specifically when $\xi_j = m_\nu^j R << 1$), the dependency on N is rather weak and the solutions for m or $n \geq 1$, can be approximated by [11, 16],

$$\lambda_k = \frac{k_{mn}}{R}\big(1 + \frac{\xi_j^2}{k_{mn}^2} - \frac{\xi_j^4}{k_{mn}^4} + ...\big). \tag{18}$$

The top panel of fig. 2 shows the plots of $S^{\alpha 0}$ as given in Eq. 17 as the function of m_1 for $N = 1$, $N = 2$ and $N = 9$ respectively for $(0,0)$ mode. It is noticed that $S_{\alpha 0}$ is close to unity when m_1 is very small as expected, however unitarity is violated with increasing m_1. The unitarity is violated by more than 5% at $m_1 = 0.05$ eV even when $N = 2$. The bottom pannel shows the similar plots for $(1,0)$ and $(1,1)$ modes respectively. As can be seen, the value of $S_{\alpha k}$ strongly depends on N at large values of m_1 even though $S_{\alpha 0}$ starts decreasing significantly with increasing N. Since $S_{\alpha k}$ is not very sensitive to N for small mass, the mixing probability $(L_j^{0k})^2$ (hence $S_{\alpha k}$) can be approximated by,

$$(L_j^{0k})^2 = \frac{2 d_k \xi_j^2}{k_{mn}^2}. \tag{19}$$

The top panel of fig. 3 shows the plot of $\lambda_k R$ as a function of m_1 for a few lowest mass states corresponding to $N = 2$. This corresponds to the case of normal torus for which $\theta = \pi/2$. The other parameter values are listed in the figure caption. For small values of m_1, $\lambda_k R$ is nearly equal to k_{mn} as expected. The ratio of the mass gaps with respect to the lowest one are $\sqrt{2}$, 2, $\sqrt{5}$, $2\sqrt{2}$ respectively. The bottom panel shows the similar plot but as a function

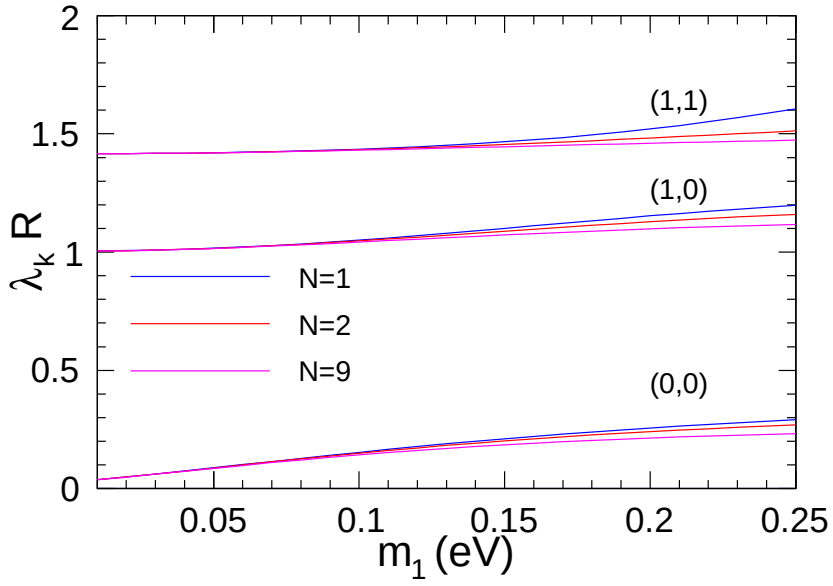

FIG. 1: The figure shows the plots of $\lambda_k R$ as a function of m_1 for $\theta = \pi/2$ and for a fixed value of $R = 3.1 \times 10^{-7}$ m. Here, k refers to the k^{th} eigen value corresponding to a given (m, n) mode. The eigen value λ_k is defined as $\frac{1}{3}\sum_j \lambda_k^j$.

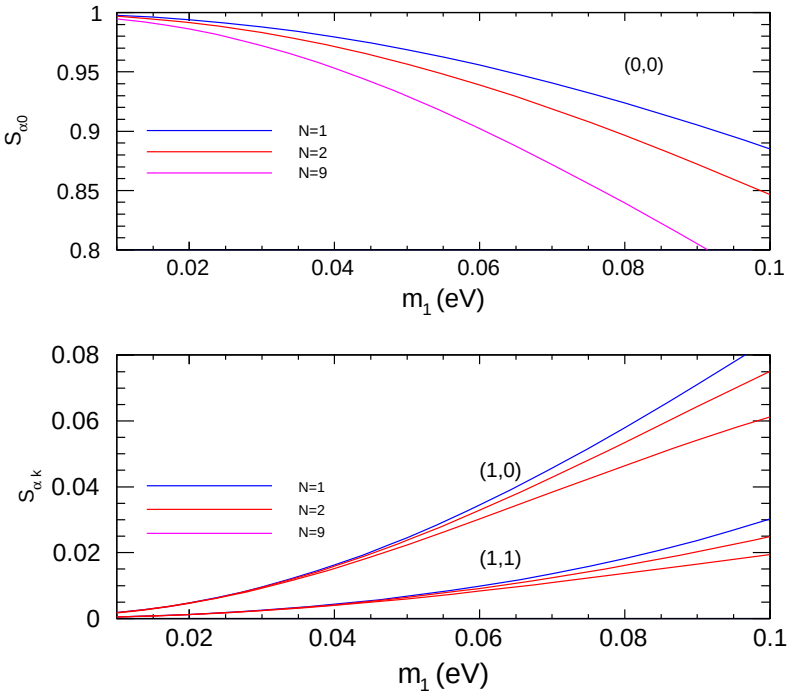

FIG. 2: The top panel shows the plots of $S_{\alpha 0}$ for $(0, 0)$ mode as the function of m_1 for $N = 1$, $N = 2$ and $N = 9$ respectively. The bottom panel shows the similar plots for $(1, 0)$ and $(1, 1)$ modes. The parameters used are same as that of fig. 1.

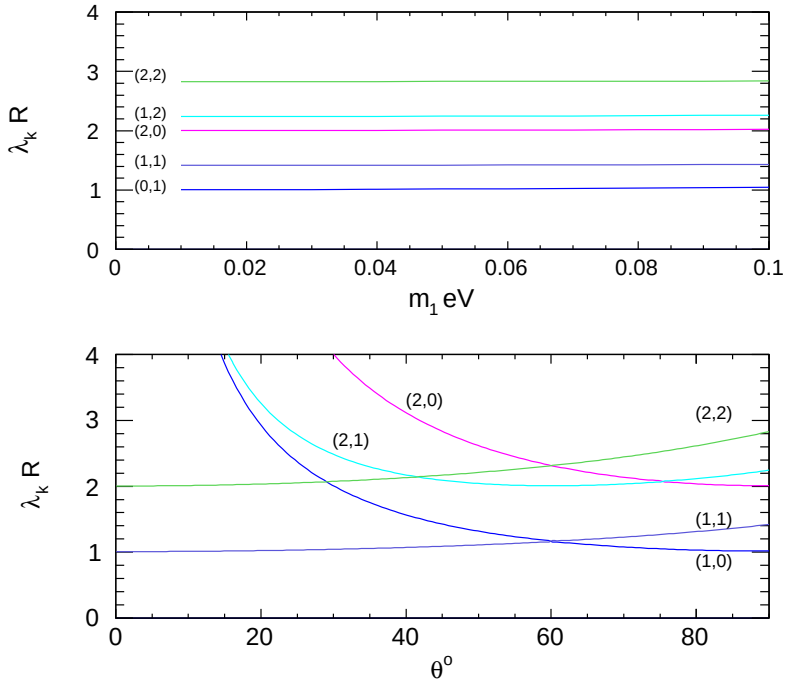

FIG. 3: The top panel shows the plots of $\lambda_k R$ as a function of m_1 for $(1,0)$, $(1,1)$, $(2,0)$, $(2,1)$ and $(2,2)$ modes corresponding to $N=2$, $\theta=\pi/2$ and $R=3.1\times10^{-7}$. The bottom panel shows the similar plots as a function of θ at a fixed mass $m_1=0.052$ eV.

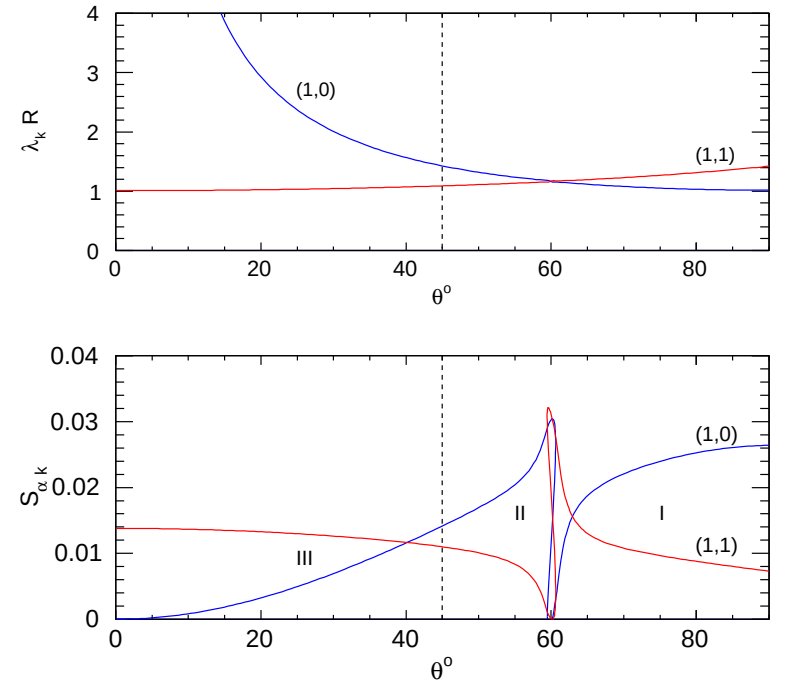

FIG. 4: The top panel shows the plot of $\lambda_k R$ as a function of θ for $(1,0)$ and $(1,1)$ modes. The other parameters are $N=1$, $m_1=0.052$ eV and $R=3.1\times10^{-7}$ m. The bottom panel shows the corrresponding $S_{\alpha k}$ as a function of θ.

of θ at a fixed mass $m_1 = 0.52$ eV. The pattern of KK mass gaps now change with decreasing θ and exhibit level crossing making some of the higher modes lighter as compared to lower ones. Although this phenomena has been studied in detail before [1, 2], we consider here only the first two mass states $(1,0)$ and $(1,1)$ which shows level crossing for $\theta < \pi/3$ which is shown more specifically in fig. 4 (see top panel). The bottom panel shows the active-sterile mixing probabilities $S_{\alpha 1}$ and $S_{\alpha 2}$ as a function of θ. In the region I, mass of $(1,1)$ mode is higer than $(1,0)$ mode and in the region III, the mass of $(1,0)$ mode is higher than $(1,1)$ mode. Accordinly, the mixing probability $S_{\alpha 1} > S_{\alpha 2}$ in region I and $S_{\alpha 2} > S_{\alpha 1}$ in region III as expected. However, the behavior is different in region II where $S_{\alpha 1} > S_{\alpha 2}$ even though the mass of $(1,0)$ mode is heavier than the mass of $(1,1)$ mode which is contrary to the naive expectation. For $\theta < 60^o$, although the mass of $(0,1)$ mode becomes higher than the mass of $(1,1)$ mode, the $(0,1)$ mode has degeneracy two times higher than $(1,1)$ mode. So the net result is $S_{\alpha 1}$ remains higher than $S_{\alpha 2}$ for small values of ξ (see Eq. 19). It can be seen that at around $\theta \sim 40^o$, the two mixing probabilities are nearly equal as the mass of $(1,0)$ mode is nearly $\sqrt{2}$ times higher than mass of $(1,0)$ mode. In general, $S_{\alpha 1} \geq S_{\alpha 2}$ in the range $40^o < \theta < 60^o$. Associating the mass of $(1,0)$ mode to Δm_{15} and mass of $(1,1)$ mode to Δm_{14} in the region II, it would mean $|U_{e5}| \geq |U_{e4}|$. This is an interesting observation indicating that there exists a range in θ where the mixing probability may become higher for havier mass and can be verified experimentally. In the present study, we have three parameters m_1, R and θ. While R decides the mass scale, m_1 controls the mixing probability and the angle θ decides the relative strength of the active-sterile coupling strength. Although, we do not optimize the above parameters to explain experimental observations, we notice that the choice of $R \sim 3.1 \times 10^{-7}$ m, $m_1 = 0.052\ eV$ and $\theta = \pi/4$ describes the experimental observations reasonably well.

TABLE I: The extracted parameters using $m_1 = 0.052$ eV and $R = 0.31 \times 10^{-7}\ m$ both for NH and IH.

Type	Angle	$\Delta m^2_{14}\ (eV^2)$	$\Delta m^2_{15}\ (eV^2)$	$\lvert U_{e4}\rvert$	$\lvert U_{e5}\rvert$
NH	90^o	0.42	0.82	0.160	0.09
IH	90^o	0.42	0.81	0.220	0.12
NH	45^o	0.48	0.82	0.105	0.120
IH	45^o	0.48	0.83	0.137	0.160

TABLE II: The $(3+2)$ global fit parameters taken from [7]. The values in first row are extracted from reactor anti-neutrino data and the values in second row are exracted from global fits.

$\Delta m^2_{14}\ (eV^2)$	$\Delta m^2_{15}\ (eV^2)$	$\lvert U_{e4}\rvert$	$\lvert U_{e5}\rvert$
0.46	0.89	0.108	0.124
0.47	0.87	0.128	0.138

In table I, we have listed a few parameters estimated at $\theta = \pi/4$ and $\theta = \pi/2$ using both normal and inverted hierachy. The estimated values are compared with the reported results which are given in the table II. The choice of $m_1 = 0.052\ eV$ results in total active neutrino mass $\sum m_\nu = 0.176$ eV which is less than the latest cosmological bound $\sum m_\nu < 0.183\ eV$ [24]. Since inclusion of sterile neutrino will exceed this upper bound, probably sterile neutrinos if present are not in thermal equilibrium in the cosmological context.

IV. FOURIER TRANSFORM OF REACTOR ANTI-NEUTRINO SPECTRA

The reactor anti-neutrino flux can be parametrized as the exponential of a fifth order polynomial valid in the range $1.8 \leq E \leq 8$ MeV [5, 6],

$$\Phi(E) = exp\left(\sum_{i=1}^{6} \alpha_i E^{i-1}\right), \tag{20}$$

where α_is are listed in table III.

The differential yield at energy E and distance L can be written as,

TABLE III: The fit parameters for various isotopes that contribute to the total power of the reactor. The parameters except for U^{238} are taken from [6] and for U^{238} from [5].

Isotope	α_0	α_1	α_2	α_3	α_4	α_5
U^{235}	4.367	-4.577	2.100	-5.294(-1)	6.186(-2)	-2.777(-3)
U^{238}	4.833(-1)	1.927(-1)	-1.283(-1)	-6.762(-3)	2.233(-3)	-1.536(-4)
Pu^{239}	4.757	-5.392	2.563	-6.596(-1)	7.820(-2)	-3.536(-3)
Pu^{241}	2.990	-2.882	1.278	-3.343(-1)	3.905(-2)	-1.754(-3)

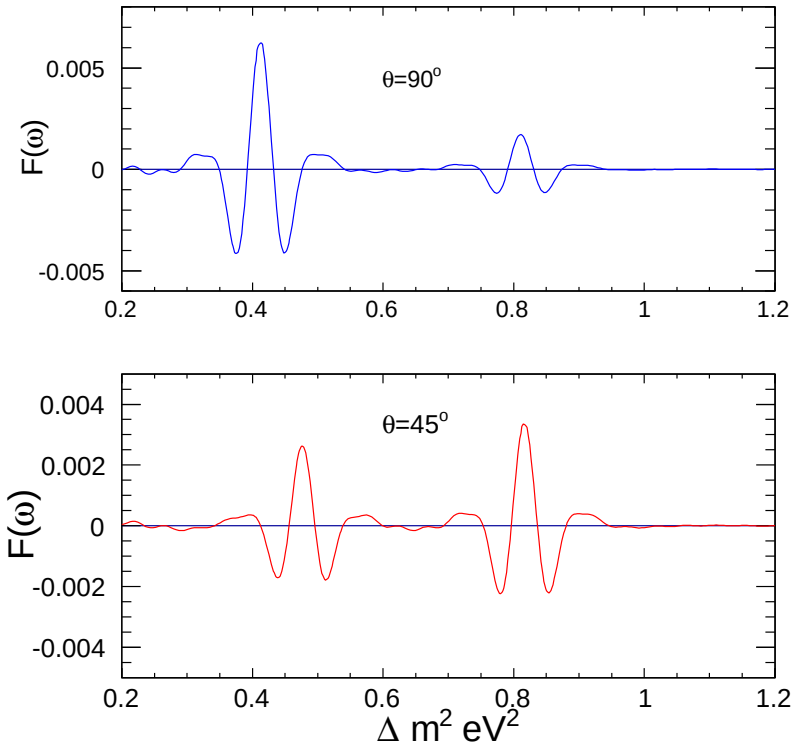

FIG. 5: The plot of the cosine Fourier transform (in arbitrary unit) as a function of Δm^2 at $\theta = \pi/2$ and $\theta = \pi/4$. The other parameters are as that of fig 4.

$$Y(L, E) = \Phi(E)\sigma(E)P_{ee}(L, E), \tag{21}$$

where E is the energy of reactor anti-neutrino, $\sigma(E)$ is the interaction cross section of anti-neutrino with matter and $P_{e,e}$ is the anti-neutrino survival probability as defined in Eq. 16. The leading order expression for the cross section of inverse-β decay ($\bar{\nu}_e \rightarrow e^+ + n$) is given by [22],

$$\sigma = 0.0952 \times 10^{-42}\ cm^2\ (E_e p_e/\ 1MeV^2). \tag{22}$$

where $E_e = E_{\bar{\nu}} - (M_n - M_p)$ is the positron energy when neutron recoil energy is ignored and p_e is the positron momentum. The fractional contributions of $U^{235} : U^{238} : Pu^{239} : Pu^{241}$ to the total power are taken in the ratio 0.538 : 0.078 : 0.328 : 0.056 respectively. We consider two sterile mass states corresponding to the parameters $m_1 = 0.052$ eV and $R = 3.1 \times 10^{-7}$ m. This corresponds to $\Delta m^2_{14} \sim 0.42\ eV^2$, $\Delta^2_{15} \sim 0.82\ eV^2$ when $\theta = \pi/2$ and $\Delta m^2_{14} \sim 0.48\ eV^2$, $\Delta^2_{15} \sim 0.82\ eV^2$ when $\theta = \pi/4$ (see table I). In order to locate the mass peak, we consider the fourier cosine transform in the $1/E$ space given by [23],

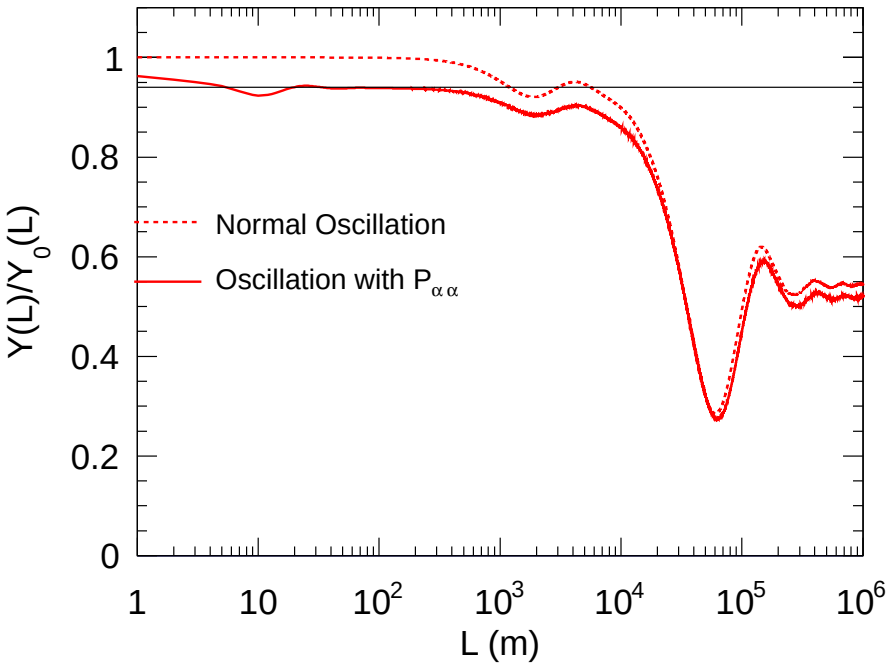

FIG. 6: The plot of the ratio of $Y(L)/Y_0(L)$ as a function of L. The dotted curve is obtained using normal oscillation parameters i.e. the probability P_{ee} is obtained without using L^{0k} factor. The solid curve is obtained using P_{ee} with L^{0k} included. This plot corresponds to $\theta = 45^o$, $R = 3.1 \times 10^{-7}$, $m_1 = 0.052$ eV with normal hierarchy. The line represents the average value at 0.94.

$$F(\omega, L) = \int_{t_{min}}^{t_{max}} \big[Y(L,t) - Y_0(E,L)\big] cos(\omega t) dt, \tag{23}$$

where $t = 1/E$ which varies from $1/E_{max}$ to $1/E_{min}$ ($E_{max} = 8$ MeV and $E_{min} = 1.8$ MeV) and ω plays the role of frequency but in units of eV. We define $Y_0(E, L)$ as the yield without P_{ee} term in Eq. 16. We have introduced Y_0 in Eq. 23 to improve the sensitivity by substracting a background term. The fig. 5 shows the cosine Fourier transform of the above spectrum as a function of $\Delta m^2 = \omega/(2.54L)$ which shows sharp peaks when $\omega \sim 2.54L\Delta m^2$. Since the active neutrino masses are nearly degenerate as compared to the sterile masses, the peaks appear at λ_{mn}^2/R^2. When $\theta = \pi/2$, the two lowest modes are $(1, 0)$ and $(1, 1)$ corresponding to mass square difference of 0.42 eV^2 and 0.82 eV^2 respectively as shown in top panel. Although $F(\omega)$ is shown in arbitray units, the height is proportional to the mixing probability. Since the height of first peak is more than the second, it would mean $|U_{14}| > |U_{15}|$. The bottom panel shows the plot when $\theta = \pi/4$ corresponding to mass square differences of 0.48 eV^2 and 0.82 eV^2 respectively. In this case, the height of the second peak is more than the first one resulting $|U_{15}| > |U_{14}|$. Although shown for $\theta = \pi/4$, it is noticed that in general $|U_{15}| \geq |U_{14}|$ in the theta range $40^o < \theta < 60^0$ even though $\Delta m_{15}^2 > \Delta m_{14}^2$.

Figure 6 shows the ratio of the total yield $Y(L)/Y_0(L)$ as a function of L in m. The dotted curve is obtained using normal oscillation probability P_{ee} which does not include the active-sterile oscillation factor L^{0k}.

The anti-neutrino survival probability is lowest when the argument in the exponential of Eq. 16 is π. This corresponds to the relation,

$$L \sim \frac{1.2E}{\Delta m^2}, \tag{24}$$

.

where we have replaced λ^2 by Δm^2. For normal oscillation, the dips occur at $L \sim 2000$ m and $L \sim 60000$ m corresponding to $\Delta m_{13}^2 = 2.42 \times 10^{-3}$ eV^2 and $\Delta m_{12}^2 = 7.45 \times 10^{-5}$ eV^2 respectively. This is consistent with the

relation given by Eq. 24 if we cnsider $< E > \sim 4$ MeV. When L^{0k} is included, another dip occurs at $L \sim 10$ m corresponding to $\Delta m^2 = 0.48\ eV^2$. The effect due to other higher masses are not significant as the mixing probability decrerases with increasing mass. The black dotted line indicates the ratio at 0.94 which is the average deficit reported in [**?**].

V. CONCLUSIONS

We have considered a toroidal extra dimensional space associated with a shape moduli characterized by an angle θ between the two large extra dimensions R_1 and R_2. The Kaluza-Klein compactification results in a tower of bulk neutrinos which couple to the active neutrinos at the brane. The active-sterile mixing probability depends strongly on the angle θ due to changing pattern of KK mas gaps resulting in level crossing. Considering only the first two KK mass states corresponding to $(1,0)$ and $(1,1)$ modes in analogy with $(3+2)$ neutrino mixing model, it is shown that there exists a range in θ ($\sim 40^o < \theta < \sim 60^o$) where the mass of the higher $(1,1)$ KK mode is lower as compared to the mass of the $(1,0)$ or $(0,1)$ mode. Since the $(0,1)$ and $(1,0)$ modes are degerate, it results in a higher active-sterile mixing probability for $(1,0)$ mode as compared to the $(1,1)$ mode. In $(3+2)$ analogy, this would mean $|U|_{e5} > |U_{e4}|$ even though $\Delta^2_{15} > \Delta^2_{14}$. This is an important observation which can be verified from the short base line neutrino measurements, although present global anlysis seems to support the above observation at $\theta \sim \pi/4$. The fourier analysis of the reactor anti-neutrino spectra at SBL also shows more qualitatively the above features which may also be possible to verify in near future with precision measurements.

[1] K. R. Dienes, Phys. Rev. Lett. **88**, 011601 (2001).
[2] K. R. Dienes and A. Mafi, Phys. Rev. Lett. **88**, 011602 (2002).
[3] N. Arkani-Hamed, S. Dimopoulos and G. R. Dvali, Phys. Lett B **429**, 263 (1998).
[4] N. Arkani-Hamed, S. Dimopoulos and G. R. Dvali, Phys. Rev. D **59**, 086003 (1999).
[5] Th. A. Muller et al, Phys. ReV. C **83**, 054615, (2011).
[6] P. Huber, Phys. ReV. C **84**, 024617 (2011).
[7] J. Kopp, M. Maltoni and T. Schwetz, Phys. Rev. Lett. **107**, 091801 (2011).
[8] J. Kopp, P. A. N. Machado, M. Maltoni and T. Schwetz, J. High Energy Physics **05**, 0501 (2013).
[9] I. Antoniadis, N. Akrani-Hamed, S. Dimopoulous and G. R. Dvali, Phys. Lett. B **436**, 257 (1998).
[10] N. Arkani-Hamed, S. Dimopoulos, G. R. Dvali and J. March-Russell, Phys. Rev. D **65**, 024032 (2002).
[11] K. R. Dienes, E. Dudas and T. Gherghetta, Nucl. Phys. B **557**, 25 (1999).
[12] G. R. Dvali and A. Y. Smirnov, Nucl. Phys. B **563**, 63 (1999).
[13] R. Barbieri, P. Creminelli and A. Strumia, Nucl. Phys. B **585**, 28 (2000).
[14] H. Davoudiasl, P. Langakker and M. Perelstein, Phy. Rev. D **65**, 105015 (2002).
[15] D. M. Gingrich, Int. Journal of Moder Physics A **24**, 5173 (2009).
[16] Q. Cao, S. Gopalakrishna and C. P. Yuan, Phys. ReV. D **69**, 115003 (2004).
[17] V. S. Basto-Gonzalez, A. Esmaili and O. L. G. Peres, Phys. Lett B **718**, 1020 (2013).
[18] W. Rodejohann and H. Zang, Phys. Lett. B **737**, 81 (2014).
[19] E. Dudas, C. Grojean and S. K. Vempati, hep-ph/051100 (2005).
[20] M. Gonzalez-Garcia, M. maltoni, J. Salvao, T. Schwetz, J. High Energy Physics **1212** 123 (2012).
[21] A. Esmaili, O. L. G. Peres and Z. Tabrizi, J. Cosmologyand astroparticle Physics **12** 002 (2014).
[22] P. Vogel and J. F. Beacom, Phy. Rev. D**60**, 053003 (1999), hep-ph/9903554.
[23] L. Zhan, Y. Wang, J. Cao and L. Wen, Phys. Rev. D**78**, 111103 (2008), hep-ex/0807.3203.
[24] E. Giusarma, M. Gerbino, O. Mena, S. Vagnozzi, S. Ho and K. Freese, astro-phi/1605.04320.

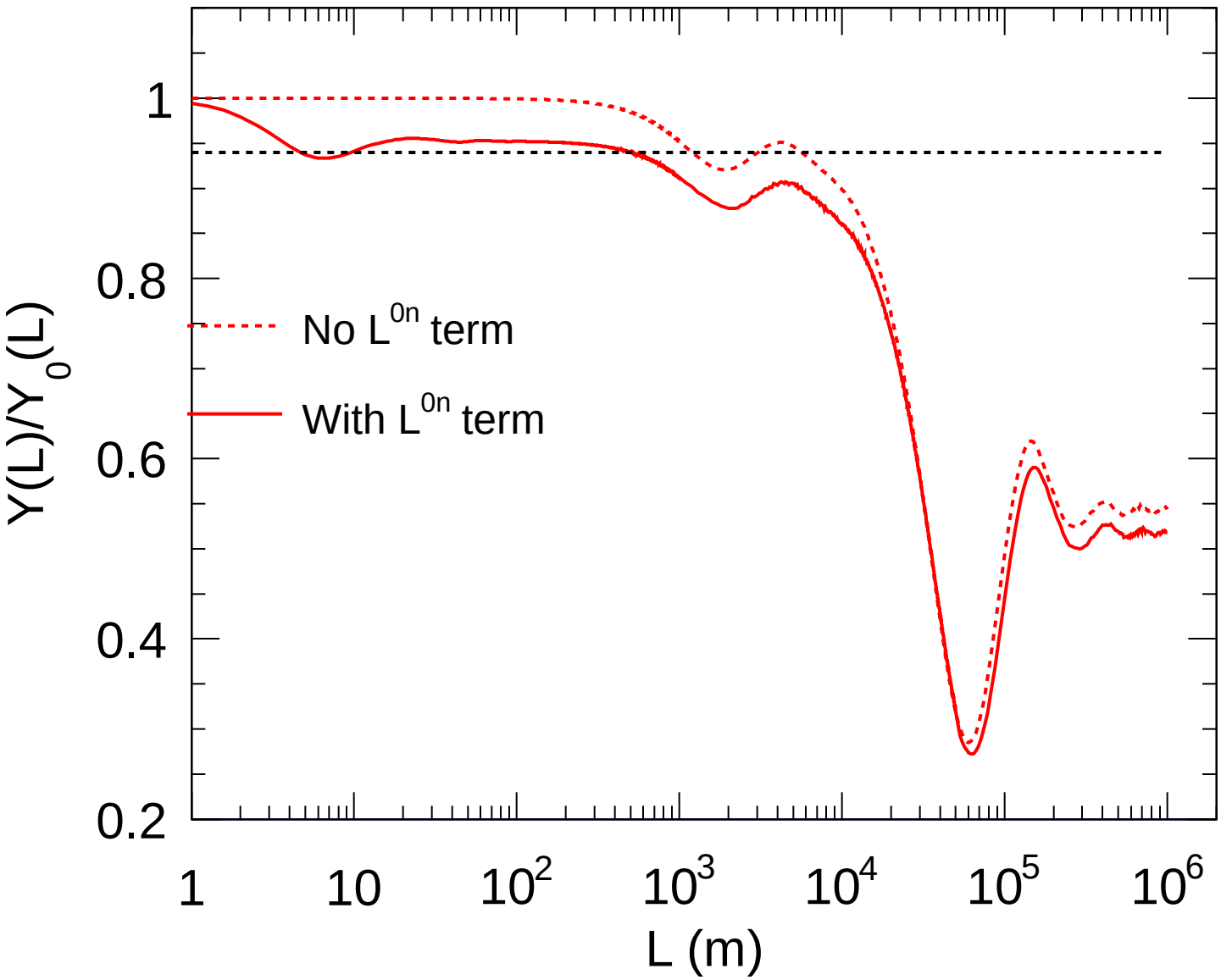
1
0.8
0.6
0.4
0.2
Y(L)/Y0(L)
No L0n term
With L0n term
1
10
10^2
10^3
10^4
10^5
10^6
L (m)